Global NEST Journal, **28** (7), 08212
Available online: 24/09/2026

The application of magnetic nanoparticles for industrial wastewater treatment using a real power plant effluent

Ali O. Imarah[1]*, Hassanin M. Ali[1], Mohammed A. Al-khafaji[2], Thamer A. Abdullah[3] and Mahmood S. Fares[4]

[1]Chemical Engineering Department, College of Engineering, University of Babylon, Babylon, Iraq.
[2]DNA Research Centre, University of Babylon, Hilla, Iraq.
[3]Applied Science Department, University of Technology, Iraq.
[4]Directorate of Electrical Energy Production, Central Region, Iraqi Ministry of Electricity, Iraq.

*Correspondence e-mail: aliumara@uobabylon.edu.iq

Abstract

Advanced wastewater treatment increasingly involves the use of nanomaterials with catalytic adsorption reactivity along with a high surface area; however, traditional nanomaterials face severe post-treatment separation difficulties, while current magnetic nanoparticles research remains largely limited to idealised synthetic water. To provide a practical alternative, this study demonstrates a novel application utilising pure commercial magnetic nanoparticles (Fe_3O_4 MNPs) to treat authentic heavy fuel oil washing wastewater generated from gas turbine operation at the Al-Khairat Power Station in Karbala, Iraq. The commercial Fe_3O_4 MNPs (20-30 nm) were characterised using Scanning Electron Microscopy (SEM) and Fourier-Transform Infrared Spectroscopy (FTIR) to verify their quality and structural integrity. A sequential batch process integrated chemical coagulation and flocculation, Fe_3O_4 MNP adsorption, and final membrane filtration. The optimal conditions were investigated, including pH and Fe_3O_4 concentration. The combined treatment significantly reduced turbidity (from 288 to 1.4 NTU). Coagulation–flocculation reduced the COD from 209 mg/L to approximately 98 mg/L, while subsequent Fe_3O_4 MNPs polishing achieved an additional reduction of approximately 50 % of the remaining COD under the optimum conditions (pH 9, 1 g/L Fe_3O_4, 90 min), translating to a cumulative overall COD removal efficiency of 76.56%. Membrane filtration successfully polished the Total Dissolved Solids (TDS) to below 500 mg/L. While the complex chemical interferences of the authentic effluent limited the maximum adsorption capacity of the nanoparticles compared to idealised synthetic models, and particle recovery poses standard operational constraints, this study proves the practical viability of using magnetic nano-adsorbents to treat high-interference industrial effluents.

Keywords: Adsorption; Flocculation; Coagulation; Contamination; Magnetic nanoparticles.

OPEN ACCESS

Received: 19/11/2025,

Accepted: 15/09/2026,

Available online: 24/09/2026

Copyright: © 2026 The Author(s). Published in Global NEST Journal. This article is licensed under the terms and conditions of the Creative Commons Attribution 4.0 International license (CC BY 4.0).

Graphical abstract

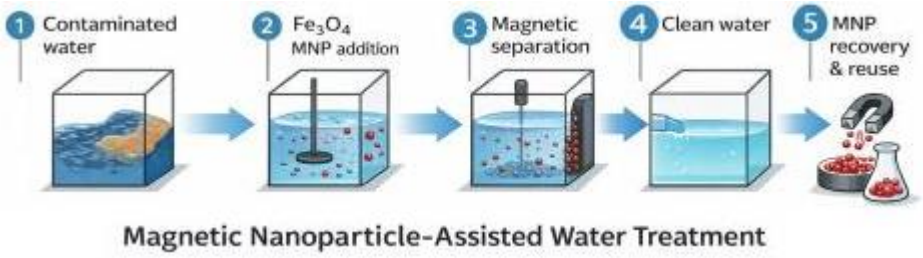

1. Introduction

Nowadays, increasing water pollution has become a major environmental challenge associated with industrial and technological development, and water and industrial wastewater treatment are at the forefront of researchers' interests (Luo *et al.*, 2021). Water and industrial wastewater contamination with toxic heavy metal ions is turning into a significant public health and environmental problem. Numerous negative consequences, including cancer, renal damage, hepatitis, miscarriages, anemia, encephalopathy, and nephritic syndrome, can be brought on by heavy metal ions (Bodzek *et al.*, 2020). Conventional methods have employed to extract and remove inorganic and organic admixtures and pollutants from water environments, including chemical precipitation, adsorption, ion exchange, membrane processes, coagulation and flocculation, flotation and extraction, irradiation, electrochemical treatment techniques, advanced oxidation, and biosorption processes (Bellona & Drewes, 2007). Moreover, nanotechnology application methods are emerging as widely applied technologies in different areas of environmental remediation due to their unique physicochemical properties (Imarah *et al.*, 2021).

Consequently, a wide range of nanomaterials is being aggressively studied for targeting hazardous metals is being studied for the extraction or removal of organic and inorganic contaminants (Abdullah *et al.*, 2023). Economically, nanotechnology helps conserve water resources and reduce energy consumption (Ali, 2012) thereby offering superior alternatives to current traditional approaches. Additionally, nano-enabled framework can be engineered to filter and use non-traditional water sources more cost -effectively (Qu *et al.*, 2013). Among these innovations, single-walled and multi-walled carbon nanotubes (CNTs) have been extensively utilized to extract and remove pollutants from water and industrial wastewater, significantly improving core physicochemical parameters such as electrical conductivity, total dissolved solids (TDS), pH, chemical oxygen demand (COD), and total organic carbon (TOC) (Babic *et al.*, 2018). With this framework, magnetic nanoparticles (MNPs) have emerged as highly efficient platforms for advanced nano-enabled water remediation (Kunduru *et al.*, 2017). MNPs, commonly referred to as iron oxide nanoparticles, consist of iron oxide core having a diameter of between 1 and 100 nm with a variety of predictable morphologies (Ansari *et al.*, 2019). Concurrently, MNPs have attracted significant attention in water and industrial wastewater treatment applications owing to their surface-to-volume ratio and rapid magnetic separation (Marcinowski *et al.*, 2020). Several studies have investigated the use of various iron oxide phases, such as maghemite (γ-Fe_2O_3), magnetite (Fe_3O_4), and hematite (α-Fe_2O_3), in the extraction/removal of heavy metals and hazardous chemicals from water and industrial wastewater, which demonstrates the performance potential of these nanomaterials (dos Santos *et al.*, 2018). Driven by these benefits, designed Fe_3O_4 MNPs were assessed in the current work as a high-capacity adsorbent specially tuned to reduce the chemical oxygen demand (COD) of authentic power plant effluent under realistic environmental interferences (Silva *et al.*, 2023).

Although Fe_3O_4 MNPs are renowned for their vast surface area and distinct magnetic characteristics, they are particularly efficient in adsorption under regulated settings. However, their direct application to complex industrial effluents often encounters major hurdles. In contrast to synthetic water models, competitive adsorption by co-existing organic fractions and heavy metal ions may prematurely saturate the nanoparticles' active catalytic sites in multi-component chemical matrices, considerably decreasing their intended efficiency (Kumar *et al.*, 2026). Furthermore, prominent challenge in standalone nano-adsorption studies involve optimizing surface charge interactions within a realistic, fluctuating pH environment. To protect the nanomaterial surface from non-targeted interferences, accelerate particle separation, and improve COD reduction, it is critical to understand the scientific synergy of combining pre-treatment stages like coagulation-flocculation with pure Fe_3O_4 nano-adsorption (Gao *et al.*, 2022; Zeng *et al.*, 2022). Despite the fact that magnetic nanoparticle-based methods for wastewater cleanup have been extensively reported in the literature, most studies performed to date are based on synthetic wastewater and controlled laboratory conditions. In this context, the present study provides an application-centered contribution to treat real industrial wastewater collected from a gas turbine power plant contaminated with a mixture of organic and inorganic pollutants. Specifically, this work evaluates the performance of an integrate coagulation–flocculation–adsorption train utilizing commercial Fe_3O_4 MNPs, followed by membrane filtration treatment under realistic operational conditions.

This multi-stage architecture aims to critically evaluate the practical viability of magnetic nanoparticles as an advanced polishing step, providing valuable thermodynamic and operational insights required to substantiate large-scale industrial implementations.

2. Materials and Methods

2.1. Chemical

All chemicals used in this study were employed as received from the supplier without any additional purification; hexane (99% purity, India), ferrous sulfate heptahydrate (99% purity, India), and polyacrylamide $(C_3H_5NO)_n$ (non-ionic, HIMEDIA, USA). Iron oxide magnetic nanoparticles (Fe_3O_4, purity >98%, particle size 20–30 nm) were obtained from US Research Nanomaterials, Inc. (Houston, TX, USA). Their morphology and particle size were characterized using Scanning Electron Microscopy (SEM), while their chemical structure and surface functional groups were analyzed using Fourier Transform Infrared Spectroscopy (FTIR). COD measurements were carried out using a COD Vario Tube Test (0–1500 mg/L, Lovibond), and analysis was performed using a Lovibond Spectro Direct photometer.

2.2. Power Plant Wastewater

The characterization of wastewater samples obtained from Al-Kharyat Power Plant Effluent was meticulously conducted in the laboratories of the Chemical Engineering Department at the University of Babylon. The detailed results are presented in **Table 1**. For measuring oil and grease content, n-hexane is used as an extractable material for non-polar materials, following EPA method 1664. Briefly, the sample pH was adjusted to 2 by adding a suitable amount of Hydrochloric acid (HCl) to 0.5 L of wastewater sample in a 1 L separatory funnel. Extraction was performed using a total of 70 mL of hexane (35 mL twice), followed by isolating the organic layer and completing the evaporation process (30 - 60 min). [24]

2.3. Coagulation and Flocculation Procedure

Following the removal of the oil and grease from the sample, 0.5 L of the prepare turbid wastewater was adjusted to initial pH value of 5 at room temperature using a suitable amount of acid or base. Ferrous sulfate heptahydrate (**$FeSO_4.7H_2O$**) was utilized as the coagulation agent at a concentration of 30 mg/L, and the mixture was flash mixed at 120 rpm for 10 minutes. Subsequently, the pH was adjusted to 6.5 at 25 °C, and the nixing speed was slowed to 50 rpm upon the addition of polyacrylamide (PAM) as a flocculation agent at a concentration of 2.5 mg/L.

2.4. Samples Analysis of Turbid Meter

The sample was placed in the magnetic stirrer device ((JOANLAB HS-17) from JOANLAB Equipment Co., Ltd. (China)), and its turbidity was determined using a calibrated turbidimeter (Lovibond, SN 10/1471, Germany), ensuring no air bubbles were present in the samples. Equation (1) can be used to get the turbidity reduction percentage (Ramavandi, 2014).

$$\text{Turbidity } R\% = \frac{\text{Turbidity}_0 - \text{CTurbidity}_f}{\text{Turbidity}_0} \times 100\% \quad (1)$$

Turbidity_0 and Turbidity_f represent the initial and final water turbidities (NTU).

2.5. Analytical Analysis

The chemical oxygen demand (COD) was measured using a thermo-reactor (DR125, Lovibond). For each experiment, 2 mL of processed wastewater was gently mixed with an oxidizing agent in a vial. The vial was then heated to 150 °C inside the reactor for 120 minutes. After cooling to room temperature, the digested sample was evaluated using a spectrophotometer (MD200, Lovibond, Germany). The COD concentration was expressed in milligrams per liter. Equation (2) was used to calculate the COD reduction efficiency (Siddiqui *et al.*, 2025). To fully optimize the polishing step performance, these evaluations were carried out systematically across all examined operational parameters, including beginning pH variations (3.0-11.0), commercial Fe_3O_4 MNPs doses (0.125-2.00 g/L), and contact time lengths (0-150 minutes). Furthermore, the COD recovery profile was monitored throughout five consecutive adsorption-desorption reusability cycles. All raw analytical COD concentration values from these various reaction setups have been extensively collated and described in **Table S1** of the Supplementary Information.

$$R\% = \frac{C_0 - C_f}{C_0} \times 100\% \quad (2)$$

Where R% is removing percent, C_0 is the initial COD concentration of COD, C_f is the final COD concentration.

2.6. Regeneration of magnetic nanoparticles

Following each adsorption cycle, the MNPs were separated from the treated effluent using an external magnetic field. To ensure the complete removal of residual contaminants, the collected nanoparticles were washed with a dilute hydrochloric acid solution (0.1 M HCl, 50 mL) under agitation for 30 min, followed by rinsing with deionized water until a neutral pH was achieved, and gentle drying at room temperature. The reusability performance and mass retention metrics of the regenerated nanoparticles was systematically evaluated over five consecutive adsorption-desorption cycles under the same operating conditions. The corresponding physical mass loss and structural capacity adjustments during this cyclical recovery sequence were thoroughly compiled and documented in **Table S3** of the Supplementary Information.

2.7. Adsorption Studies

The batch adsorption tests were conducted with continuous magnetic stirring at 200 rpm at room temperature (25 ± 2 °C). By systematically varying the starting pH (3.0–11.0) and contact duration (0–150 min), the optimization of operating parameters was examined. The system attained adsorption equilibrium after a contact duration of 90 minutes, and the ideal pH was determined at 9.0 based on the experimental profiles. Equilibrium mass balance and isotherm models were used to examine the experimental results. The equilibrium adsorption capacity q_e (mg/g), representing the amount of Chemical Oxygen Demand (COD) adsorbed per unit mass of MNPs at

equilibrium, was determined using the following mass balance equation:

$$qe = \left(\left(Co - Ce \right) * V \right) / m \quad (3)$$

Where C_o is the wastewater's original COD content prior to MNP treatment (98.0 mg/L), Ce is the equilibrium residual COD concentration (mg/L) remaining in the solution following treatment. V is the volume of the wastewater sample (L). m is the mass of the Fe_3O_4 MNPs added (g). Under the optimized constraints, where the equilibrium removal efficiency reached 50.0% and the ideal adsorbent dosage was established at 1.0 g/L (maintaining a V/m ratio of 1 L/g), the residual equilibrium concentration (Ce) was computed as follows:

$$Ce = C_0 \times \left(1 - \frac{Re\ \%}{100} \right) = \left(98 \times 0.5 \right) = 49\, mg / L \quad (4)$$

Thus, the experimental adsorption capacity (qe) at the optimum boundary was determined to be:

$$qe = \frac{(C_0 - Ce) \times V}{m} = \frac{(98 - 49) \times 1}{1} = 49 \frac{mg}{g} \quad (5)$$

$$Ce / qe = \frac{1}{qmax\ .K} + \frac{Ce}{qmax} \quad (6)$$

Where q_{max} is the theoretical maximal monolayer adsorption capacity (mg/g), and (K) is the Langmuir affinity constant (L/mg) associated with the adsorption's free energy. The observed plateau in COD removal efficiency at higher Fe_3O_4 MNPs dosages suggest progressive saturation of the available adsorption sites, which is highly consistent with Langmuir-type monolayer adsorption concept. To quantitatively support the results, the linear Langmuir equation (Eq. 6) was fitted with the ideal boundary equilibrium parameters (Ce = 49.0 mg/L and qe = 49.0 mg/g). By constraining maximum monolayer capacity (q_{max}) to the total available pollutant load (98.0 mg/g) based on saturation trajectory. the Langmuir affinity constant (K) was mathematically resolved as 0.0204 L/mg, confirming a favorable interaction matrix under the optimized alkaline conditions.

Moreover, Kinetic modeling was applied to the experimental data in order to elucidate the adsorption mechanism and identify the rate-limiting step of the reaction. The reaction mechanism represented in Equation (7) was assessed using the linear form of the pseudo-First-order kinetic model, which exhibited a highly reliable statistical alignment (R^2=0.9701) with the experimental dataset.

$$\ln q_{e-} q_t = \ln q_e - K1 \times t \quad (7)$$

where k_1 is the pseudo-first-order rate constant (min^{-1}) and qt is the quantity of COD adsorbed (mg/g) at time t (min).

2.8. Statistical Analysis

To ensure methodological transparency and data reproducibility, each experimental run (coagulation, analytical mesurments, adsorption, and Fe_3O_4 NPs regeneration) was carried out in triplicate (n = 3). The quantitative values are presented as mean ± standard deviation (SD). All experimental data were subjected to a one-way analysis of variance (ANOVA) using OriginLab (Version 2024) and Microsoft Excel in order to verify the statistical rigor. The threshold for statistical significance was set at $p < 0.05$.

3. Results and Discussion

3.1. Fe_3O_4 NPs Characterization

The surface morphology and particle size of iron oxide were characterized using SEM instrument, as seen in **Figure 1**. The SEM measurements exhibited spherical or quasi-spherical shapes with significant aggregation. This agglomeration is commonly related to the magnetic characteristics of iron oxide, and it is thought to be a typical behavior caused by magnetic dipole-dipole attractions among nanoparticles.

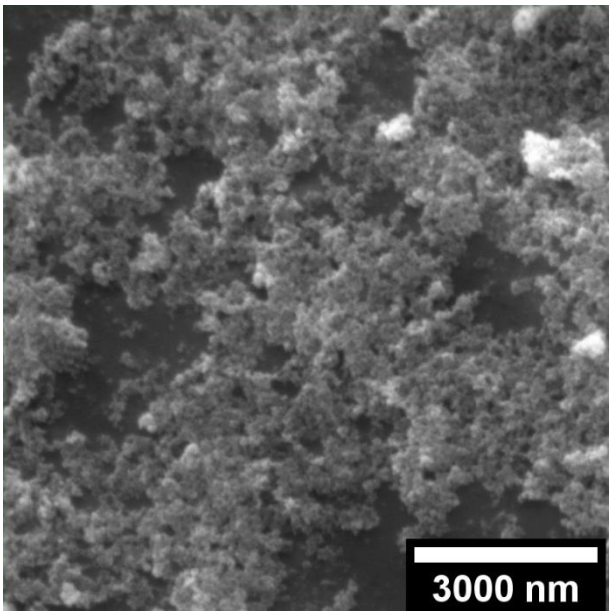

Figure 1. SEM micrograph of the iron oxide nanoparticles

The SEM analysis revealed that the particle size of the nanoparticles ranged from 20 to 50 nm, as determined using ImageJ software, which included data from over 100 particles. The chemical structure of iron oxide nanoparticles was also determined using FTIR spectroscopy, as seen in **Figure 2**. The spectrum reveals a high absorption peak at 573 cm^{-1}, attributable to the Fe-O stretching vibration (T. Yang *et al.*, 2024). **Figure 2** also shows a broad OH stretching band at the range of 3410–3440 cm^{-1}, indicating the presence of surface hydroxyl groups. The broad breadth of this band is due to the intermolecular or intramolecular hydrogen bonding of O-H groups with adsorbed water molecules. Furthermore, the deformation (bending) vibration band of H_2O associated with the -OH group is found about 1637 cm^{-1} (Al-Khafaji *et al.*, 2022).

3.2. FTIR analysis and adsorption evidence

FTIR measurements of Fe_3O_4 NPs were also used to assess pollutant elimination. **Figure 2** displays the spectrum of Fe_3O_4 magnetic nanoparticles after wastewater treatment, and the results revealed that anew absorption bands appear in the treated sample that are absent from the

untreated sample which is a sign of interaction between organic pollutants and surface of nanoparticles. The bands located near 2871 cm^{-1} are related to C–H stretching vibrations of aliphatic group (CH_3 and CH_2) which indicates the existence of organic compounds attached on these nanoparticles. In addition, the appearance and increased intensity of broad bands in the range of 3410–3440 cm^{-1} are associated with O–H stretching vibrations of the surface hydroxyl groups on Fe_3O_4 and adsorbed water molecules or oxygen-containing organic species. These changes indicate that hydrogen bonding and surface interactions play an important role in the adsorption process. Although FTIR analysis does not allow precise identification of individual pollutants, the observed spectral changes provide qualitative evidence supporting the adsorption of organic contaminants onto the magnetic nanoparticle surface rather than chemical transformation of the compounds (Al-Khafaji, 2023).

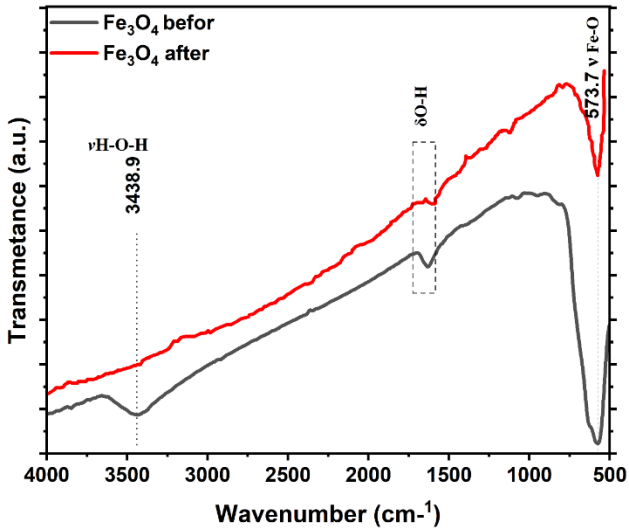

Figure 2. FTIR spectra of Fe_3O_4 NPs before and after removal pollutants.

It is important to keep in mind that the Fe_3O_4 MNPs used in this study were provided by reliable commercial suppliers, ensuring that the original physical properties were maintained. SEM and FTIR analyzes were used in quality-control procedures to ensure structural purity and confirm that the particle sizes and surface functional groups matched nano-scale dimensions. The experimental FTIR vibrational bands and SEM clustered patterns showed good alignment with conventional literature, confirming the material's integrity. As a result, no additional baseline physical profile is necessary for this optimization inquiry.

3.3. Pre-treatment efficiency before MNP application

The effectiveness of the extraction and removal process is illustrated in **Figures 3** (A) and (B). N-hexane was used as an extractant for non-polar substances following EPA method 1664. This step resulted in a distinct two-phase separation where the organic layer successfully removed oil and other organic compounds from the aqueous phase. Following the evaporation of n-hexane, the remaining oil and solid content were measured.

The remaining aqueous phase was then subjected to coagulation using ferrous sulfate heptahydrate (30 mg/L) for 10 minutes at room temperature, as shown in **Figure 3** (C), primarily to target the suspended solids. Subsequent flocculation (**Figure 3 (**D)) significantly reduced turbidity from 288 NTU to 1.4 NTU, further enhancing the removal of suspended solids and residual oil. As a result, these pre-treatment steps decreased the chemical oxygen demand (COD) from 209 mg/L to about 98 mg/L, indicating that coagulation–flocculation is responsible for removing most of the suspended solids and a large portion of the COD. Finally, Fe_3O_4 MNPs were applied as a polishing step, focusing on the removal of residual dissolved organic contaminants that are not effectively eliminated during pre-treatment, and achieving an additional COD reduction of approximately 50% relative to the remaining COD.

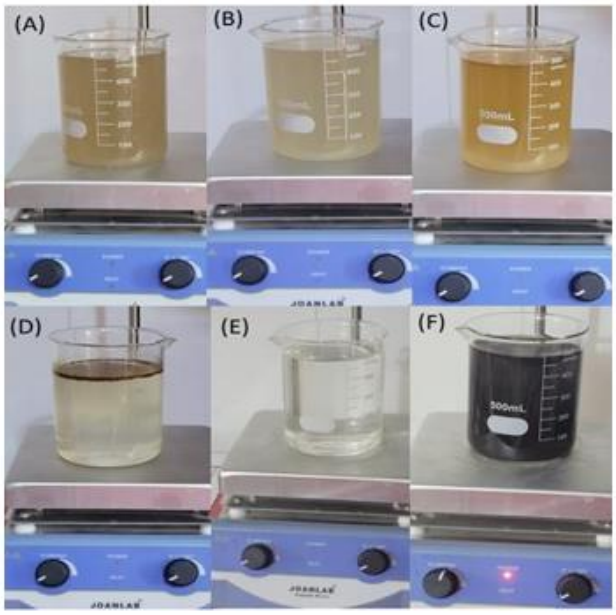

Figure 3. Wastewater treatment process: (A) Effluent water, (B) After n-hexane treated, (C) Coagulation process with ferrous sulfate, (D) Flocculation with polyacrylamide, (E) Water filtration, and (F) COD reduction using MNPs, all the process was at room temperatures (25 ^{o}C).

3.4. Effect of pH on COD removal.

The COD removal efficiency was significantly affected by the pH value. Under acidic conditions,an excess H^+ ions competed with organic pollutants for adsorption sites on MNPs surface which resulted in lower removal efficiency of the process (K. Yang *et al.*, 2026). This competition decreased when pH in a row close to neutral as well as feebly alkaline problems, thereby accelerating adsorption from the solution. As a result, the poorer adsorptive capacity and weaker bonding in weakly acidic conditions were strategically used to backwash the nanocomposite. This method efficiently desorbed the bound contaminants, making it easier to regenerate and reuse the nanoparticles in subsequent water treatment cycles. The maximum COD removal (~49%) was measured at pH 9, where the adsorption of pollutants was facilitated by improved electrostatic interactions and reduced pollutant solubility. Efficiency decreased slightly at higher pH values (>9), which could be attributed to varying pollutant speciation and

lower adsorptive affinities. All experiments were performed in triplicate (n = 3). Values are indicated as mean ± 0.5 % standard deviation, see **Figure 4** (A).

3.5. Effect of MNPs concentration.

The concentration of nanoparticles was also discovered to play a major influence in the efficacy of contaminant removal. Increasing the MNP dosage from 0.125 to 1 g/L markedly improved the COD removal by providing a greater number of adsorption sites. Beyond 1 g/L, removal effectiveness plateaued at roughly 50 %, implies a progressive saturation trend of the finite available adsorption implies a progressive saturation trend of the finite available adsorption. Such behavior is in agreement with surface-limited adsorption phenomena having been previously observed in analogous Fe_3O_4-based wastewater treatment studies (Tlili *et al.*, 2023), which subsequently demonstrates **Figure 4** (B).

3.6. Effect of contact time

The rapid initial COD removal rate was observed during the first 80 min, driven by the abundance of vacant active sites and a strong concentration gradient. Following this period, the removal efficiency attained a plateau, suggesting that adsorption equilibrium was reached. As shown **Figure 4** (C), extending the contact time beyond this equilibrium point yielded negligible further removal. This behavior confirms that under the studied conditions, process performance is primarily governs by the saturation of surface-active sites rather than kinetic limitations.

3.7. Reusability of magnetic nanoparticles

The reusability of MNPs was also investigated, with the results displayed in **Figure 4** (D). The results showed that, while a high initial COD removal effectiveness was attained, it gradually decreased over subsequent cycles, reaching around 18.0 % after the fifth cycle. This performance decay is hypnotically attributed to potential surface fouling induced by the irreversible deposition of organic pollutants, insufficient regeneration during the diluted acid backwashing phases, and the subsequent blockage of active adsorption sites.

Concurrently, this operational degradation is likely amplified by a gradual cumulative mass loss, which reached an estimated 13.5% by the fifth run, as shown in **Table S3** of the Supplementary Information. This mass loss, mostly induced by partial acid dissolution and processing erosion, results in continual nanoparticle aggregation over repeated uses, limiting the net effective surface area available for late-stage cycles. Nonetheless, our findings indicate that magnetic nanoparticles have substantial potential for recurrent industrial application, notwithstanding their poor late-stage performance. Enhancing regeneration strategies, such as thermal optimization or targeted chemical activation, may aid in the retention of adsorption activity across several cycles. To place the achieved COD removal performance in context, a quantitative comparison with selected Fe_3O_4-based wastewater treatment studies reported in the literature is presented in **Table 2**. The comparison focuses on key operating parameters, including wastewater type, Fe_3O_4 dosage, pH, contact time, and COD removal efficiency. This comparison highlights the relevance of the present results obtained using real industrial wastewater.

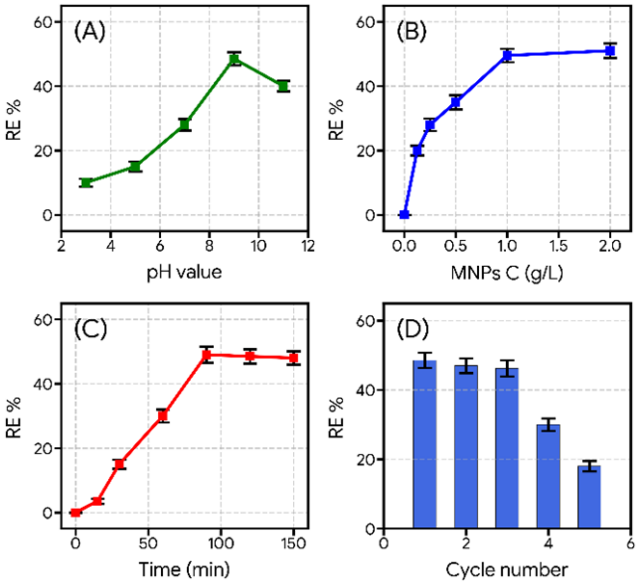

Figure 4. illustrates the factors affecting Chemical Oxygen Demand (COD) removal through the following: (A) the initial pH ranging from 3 to 11, which shows variability in COD removal efficiency at a constant stirring speed of 200 rpm, with a dosage of 1 g/L of magnetic nanomaterials (MNPs) over a time frame of 90 minutes; (B) the impact of MNP dosage variations between 0.125 to 2 g/L, evaluated at a consistent contact period of 90 minutes; (C) the dependence of COD removal on different contact times, spanning from 15 to 150 minutes, while maintaining a MNP dosage of 1 g/L; and (D) the assessment of MNPs' reusability across five successive cycles. Error bars represent the standard deviation of independent triplicate measurements (n = 3).

The study evaluated the efficiency of Fe_3O_4 nanoparticles in lowering COD in actual power plant effluent, and the results were consistent with earlier findings, such as those by (Tetteh & Rathilal, 2021), who reported a 55% COD reduction at a dose of 1.0 g/L. This performance is also within the ranges reported by Marcinowski and Mateus, who demonstrated reductions ranging from 40% to 65%. The nanoparticles demonstrated effective COD removal under alkaline conditions (pH 9.0), which is a significant advantage over acidic surroundings (pH <4.0) (Marcinowski *et al.*, 2020; Mateus *et al.*, 2020). This stability in alkaline conditions is hypnotically attributed to the nanoparticles' engineered commercial magnetite surfaces, which retain useful binding sites for organic pollutants while neither losing charge or precipitating iron. Furthermore, the study addressed the complexity of actual wastewater, whereas previous studies have frequently focused on synthetic matrices with better COD removal rates. While studies by Dağdaş et. al. and Yang et. al. used sophisticated frameworks to obtain over 80% removal, our study shows that Fe_3O_4 nanoparticles perform effectively under complex real industrial wastewater conditions at a modest dose of 1.0 g/L (Dağdaş Kaya & Öztürk, 2026; T. Yang *et al.*, 2024). The nanoparticles' capacity to reduce COD by approximately 50.0 % without requiring additional co-

catalysts implies their structure viability and selectivity for industrial applications.

Table 1. Physio-chemical properties of the processed wastewater and their respective target specifications.

No	Quality parameter	Units	Effluent value	Target
1	Temperature	℃	70	<35 C
2	pH	--	7.8	6-9
3	TDS	mg/L	6000	<500
4	TSS	mg/L	263	<60
5	Turbidity	NTU	288	<10
6	COD	mg/L	209	<100
7	Conductivity	mS/cm	28.8	<-
8	Oil component	mg/L	214	0

Table 2 Quantitative comparison of Fe_3O_4-based wastewater treatment studies for COD removal

Study	Wastewater Type	Fe_3O_4 Dosage (g/L)	pH	Contact Time (min)	COD Removal (%)
[(Zakrzewski *et al.*, 2021)]	Synthetic dye wastewater	0.5–1.5	7.0–9.0	60–120	45–65%
(Marcinowski *et al.*, 2020)	Cosmetic wastewater	0.8–1.2	7.0–9.0	60	40–60%
(Li *et al.*, 2021)	Oilfield Produced Water	1.5	7.0	60	66.7% (Fe_3O_4-IDA-Cu2+)
(Tetteh & Rathilal, 2021)	Textile effluent	1.0	8.0	90	~55%
(T. Yang *et al.*, 2024)	Oil Field Produced Water	2.0	5.0	10	90.44%
(Dağdaş Kaya & Öztürk, 2026)	Synthetic Textile Dye Solutions	80.0	7.4	35	up to 84% (Biochar matrix)
Present study	Real power plant wastewater	1.0	9.0	90	~50%

3.8. Discussion of the adsorption isotherm, kinetics, and mechanism

To further understand the interaction between organic pollutants (COD) and the MNP surfaces, the adsorption equilibrium and mechanism were evaluated. All experimental COD values measured under the various operational factors investigated in this study have been compiled and listed in **Table S1** of the Supplementary Information. The experimental parameters and equilibrium adsorption capacity data were evaluated using equilibrium isotherm and rection kinetic models. The derived parameters for both the adsorption isotherm and reaction kinetics, along with the linear plotting data, have been thoroughly documented in **Table S2** of the Supplementary Information. The experimental dose-response curve (Fig. 4B) demonstrated that the COD removal efficiency plateaued at approximately 50.0% when the Fe_3O_4 MNP dosage reached 1.0 g/L. This distinct plateau behavior implies progressive saturation of a finite number of active surface sites, which is highly consistent with monolayer adsorption concepts. To verify this behavior, the linear form of the Langmuir adsorption isotherm was applied directly to the optimal boundary state equilibrium constraint obtained from wastewater matrix as explained in Section 2.7, Eq. 6. By constraining the boundary conditions, it was found that the theoretical maximal monolayer adsorption capacity (q_{max}) was 98.0 mg/g. At the same time, the adsorption free energy-related Langmuir affinity constant (K) was determined to be 0.0204 L/mg. Under the intended alkaline environment, this mathematical approximation suggests a very favorable and stable affinity between the magnetic nanoparticle surfaces and organic pollutants in industrial wastewater.

The transient data displayed in Fig. 4C showed a high initial COD elimination rate during the first 60 minutes, driven by the strong concentration gradient and an abundance of unoccupied active functional sites, before falling into a tight equilibrium plateau at 90 minutes with an experimental capacity (q_{e_exp}) of 49 mg/g. To understand the underlying rate-limiting process, the pseudo-first-order kinetic model was incorporated into the empirical investigation via its standard linear expression, as shown in Section 2.7, Eq. 7. The resulting linear regression plot for the pseudo-first-order kinetic model has been integrated into Figure S1 of the Supplementary Information. Kinetic processing yielded a calculated equilibrium capacity (q_{e_cal}) of 53.37 mg/g, with a strong statistical correlation (R^2 > 0.9701) with the experimental profile. The rate constant (k_1) was determined as 0.0171 min^{-1}. This solid alignment with pseudo-first-order kinetics suggests that physical mass transfer limitation, film diffusion, or external boundary layer resistances govern the primary rate-controlling mechanism, during the early stage of the COD adsorption process. Without direct measurements of surface charge or interfacial chemistry, the adsorption mechanism remains a tentative conceptual framework. At an optimal pH of 9.0, the process is consistent with pseudo-first-order kinetics and FTIR shifts, showing that physical

mass transfer and resistance considerations are the primary influences. Secondary interactions, such as potential weak electrostatic forces, hydrogen bonding, or surface coordination, may potentially be involved, but require further investigation for validation. A unique separation between the cumulative output and the individual stage efficiencies was made in order to fully explain the sequential performance of the integrated treatment system. The raw influent COD was lowered from 209.0 mg/L to an intermediate level of 98.0 mg/L during the first coagulation–flocculation pre-treatment phase, resulting in a primary removal efficiency of 53.11%. The residual organic load was then the focus of the secondary Fe_3O_4 MNP advanced polishing stage, which further reduced the concentration from 98.0 mg/L to a final effluent value of 49.0 mg/L, indicating a 50.0% solo polishing-step efficiency. When combined throughout the whole integrated cycle, the sequential process produced a cumulative total COD removal efficiency of 76.56%, proving that primary chemical sedimentation and magnetic nanomaterial adsorption may work in concert.

Lastly, when it comes to long-term operational viability, cyclic performance and mass retention boundaries must be taken into account. To comprehensively monitor these trends, the standalone adsorption capacity (qe), regeneration efficiency (%), nanoparticle recovery (%), and cumulative mass loss (%) across five successive runs were systematically evaluated and documented in **Table S3** of the Supplementary Information. Over the course of the first three successive adsorption-desorption cycles, the regenerated MNPs demonstrated extremely consistent stability, maintaining strong COD removal efficacy (46.2%–48.5%) as shown in Fig. 4D, with corresponding capacity values ranging between 45.28 and 47.53 mg/g, reflecting a remarkable regeneration efficiency above 95.25%. But in the fourth and fifth runs, removal capacity dropped sharply to 30.0% and 18.0%, respectively, as performance collapsed. In real power plant effluent, complex, macromolecular organic contaminants cause irreversible chemisorption or steric hindrance across several cycles, leaving localized active sites permanently occluded despite diluted acidic washing (0.1 M HCl). The total nanoparticle recovery percentage decreased from 98.2% in Cycle 1 to 86.5% by Cycle 5, indicating that this operational failure is physically exacerbated by a gradual mass loss. The main causes of this estimated 13.5% cumulative mass loss include physical transfer erosion, partial acid dissolution during regeneration, and nanoparticle agglomeration, which significantly limits the net effective surface area available for late-stage cycles. The real-world fouling and physical handling limits reported for magnetic nanomaterial matrices in industrial wastewater treatment are highly consistent with our findings (Aali *et al.*, 2025; Edet & Ifelebuegu, 2020; Waleed Juma *et al.*, 2026).

3.9. The final stage of the treatment process.

The final stage of the sequential wastewater treatment was reduction of Total Dissolve Solid (TDS) via membrane filtration. Following the removal bulk pollutants through coagulation–flocculation and magnetic nanoparticle polishing, the effluent was transferred by diaphragm pump (SML-8806). Despite the successful removal of turbidity and COD in the previous steps, the treated water still exhibited a high TDS concentration, fluctuating within the range of almost 5000–6000 mg/L. Thus, a commercial membrane purification system (Pure Studio Purifier Membrane, PS-1812075) was integrated as an additional post-treatment polishing step. Operating under reverse osmosis (RO) principles, the semi-permeable membrane selectively separates water molecules while the membrane's active layer rejects the dissolved salts and ions under applying pressure (see **Figure 5**). Membrane filtration was performed at room temperature in accordance with manufacturer's operating conditions and the permeate from each treatment effluent was continuously supplied to the membrane unit. This step was mainly focused on the removal of dissolved salts rather than suspended or organic pollutants. Finally, the final membrane filtering step effectively decreased the TDS content to less than 500 mg/L, reaching the average threshold values set by local environmental release and water reuse requirements.

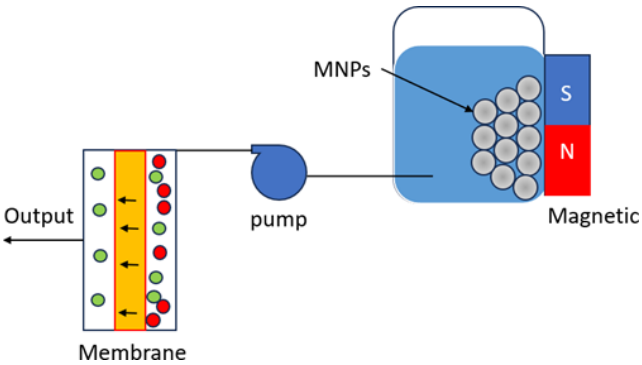

Figure 5. Last process used for decreasing the TDS from 5000 to < 500 mg/L.

4. Conclusions

This study demonstrates that a combination of coagulation–flocculation followed by Fe_3O_4 MNPs adsorption and membrane filtration can effectively purify real industrial wastewater. Following the application of the optimized conditions established in this work (pH 9, 1 g/L MNP dosage, and contact time of 90 min), effluent turbidity drastically decreased from 288 NTU to 1.4 NTU primary coagulation–flocculation pre-treatment stage successfully reduced the initial raw wastewater COD concentration from 209.0 mg/L down to an intermediate level of 98.0 mg/L, translating to a standalone chemical sedimentation efficiency of 53.11%. This integration ensured that a substantial organic fraction was removed before going through nanoparticles treatment process. The secondary Fe_3O_4 MNP polishing stage reduced COD to 49.0 mg/L, achieving a single polishing-step efficiency of around 50.0%. When combined with the whole continuous operational train, the sequential process achieved a cumulative total COD elimination efficiency of 76.56%. This polishing performance is highly comparable to the efficiency thresholds reported in previous Fe_3O_4-based literature (40–70%). However, unlike most previous investigations conducted using synthetic wastewater

under controlled laboratory conditions, the present study evaluated real power plant wastewater containing complex organic and inorganic contaminants. The actual power plant effluent used in this investigation had substantial organic and inorganic interferences. Furthermore, it was demonstrated that MNPs function very well at pH 9, which is hypothetically imply attributed to more favorable adsorption interactions in settings that are somewhat alkaline. Furthermore, falling returns above a dosage of 1.0 g/L MNP strongly imply a progressive saturation trend of the finite available adsorption sites, meaning that increasing the adsorbent mass above this threshold does not yield corresponding benefits in COD removal. The recommended MNP-based treatment plan considers both economic and practical aspects. They can be efficiently separated under an external magnetic field, eliminating time-consuming procedures like filtering or centrifugation and requiring less energy than pressure-driven methods. While MNPs are more costly than standard coagulants, which limits their usage as a standalone solution, they are effective as a polishing step after coagulation-flocculation, lowering the amount of material and dose necessary. A number of limitations are also worth mentioning. The experiments in this phase were performed in a batch mode, which may not fully simulate continuous industrial operation. Furthermore, kinetic modeling of the transient data indicated that the adsorption trajectory was limited by physical transport limits, displaying reliable linear compatibility with the Pseudo-First-Order model (R^2 = 0.9701, k_1 = 0.0171 min^{-1}). After five cycles of reusing the nanoparticles, the removal effectiveness gradually decreased to around 18.0%. This performance degradation is severely analyzed in our additional profiles as a result of both localized chemical active site blockage and an estimated 13.5% cumulative physical mass loss caused by repetitive acid washing (0.1 M HCl) and handling erosion. Lastly, a detailed estimation of techno-economical parameters like the cost of nanoparticles, regeneration efficiency, energy consumption and large-scale operation feasibility are out of the scope of this work. These features are key limitations that should be targeted in further investigations. It is suggested that future work should be directed towards continuous-flow operation, better regeneration strategies, adsorption mechanism studies and techno-economic life-cycle assessments with the aim of substantiating large-scale industrial implementation.

Funding

The authors declare that no funds, grants, or other support were received during the preparation of this manuscript.

Conflict of interest

The authors declare no competing interests.

References

Aali, R., Azari, H., Pasalari, H., Yaghmaeian, K., Yousefi, M., Azari, A., Yari, A. R., Sharifi, N., Kamani, H., & Dowlati, M. (2025). Enhanced sulfadiazine degradation through synergistic visible light assisted peroxymonosulfate activation using a magnetic Fe_3O_4-$ZnIn_2S_4$ catalyst. *Scientific Reports*, *15*(1), 25013. https://doi.org/10.1038/s41598-025-10973-4

Abdullah, T. A., Rasheed, R. T., Adnan, M., Qasim, B., Sajet, F., Mansoor, H. S., Talib, H., Kadhim, M. S., Kułacz, K., Meharban, F., & Abdul-Zahra, Z. (2023). A comprehensive review of the application of modified carbon nanotubes (CNTs) for the removal of metals from wastewater. *Materials Research Express*, *10*(12), 122005. https://doi.org/10.1088/2053-1591/ad1770

Ali, I. (2012). New generation adsorbents for water treatment. *Chemical Reviews*, *112*(10), 5073–5091. https://doi.org/10.1021/cr300133d

Al-Khafaji, M. A. (2023). *Preparation and surface modification of porous hollow organosilica particles for biomedical applications* [Eötvös Loránd Tudományegyetem]. https://doi.org/10.15476/ELTE.2022.076

Al-Khafaji, M. A., Gaál, A., Jezsó, B., Mihály, J., Bartczak, D., Goenaga-Infante, H., & Varga, Z. (2022). Synthesis of Porous Hollow Organosilica Particles with Tunable Shell Thickness. *Nanomaterials*, *12*(7), 1172. https://doi.org/10.3390/nano12071172

Ansari, S. A. M. K., Ficiarà, E., Ruffinatti, F. A., Stura, I., Argenziano, M., Abollino, O., Cavalli, R., Guiot, C., & D'Agata, F. (2019). Magnetic Iron Oxide Nanoparticles: Synthesis, Characterization and Functionalization for Biomedical Applications in the Central Nervous System. *Materials*, *12*(3), 465. https://doi.org/10.3390/ma12030465

Babic, B., Calatayud, M. P., & Cvjetic, N. (2018). *Journal of Magnetism and Magnetic Materials Magnetic and power absorption measurements on iron oxide nanoparticles synthesized by thermal decomposition of Fe (acac) 3*. *449*, 286–296. https://doi.org/10.1016/j.jmmm.2017.10.053

Bellona, C., & Drewes, E. Ã. (2007). *Viability of a low-pressure nanofilter in treating recycled water for water reuse applications: A pilot-scale study*. *41*, 3948–3958. https://doi.org/10.1016/j.watres.2007.05.027

Bodzek, M., Konieczny, K., & Kwiecińska-Mydlak, A. (2020). The application of nanomaterial adsorbents for the removal of impurities from water and wastewaters: A review. *Desalination and Water Treatment*, *185*, 1–26. https://doi.org/10.5004/dwt.2020.25454

Dağdaş Kaya, E., & Öztürk, D. (2026). Enhanced organic removal from landfill leachate via heterogeneous electro-fenton process using ternary Fe3O4/Co3O4/CuO-rGO catalyst: RSM-based numerical optimization. *Chemical Engineering Research and Design*, *231*, 115–130. https://doi.org/10.1016/j.cherd.2026.06.006

dos Santos, T. R. T., Silva, M. F., de Andrade, M. B., Vieira, M. F., & Bergamasco, R. (2018). Magnetic coagulant based on moringa oleifera seeds extract and super paramagnetic nanoparticles: Optimization of operational conditions and reuse evaluation. *Desalination and Water Treatment*, *106*, 226–237. https://doi.org/10.5004/dwt.2018.22065

Edet, U. A., & Ifelebuegu, A. O. (2020). Kinetics, Isotherms, and Thermodynamic Modeling of the Adsorption of Phosphates from Model Wastewater Using Recycled Brick Waste. *Processes*, *8*(6), 665. https://doi.org/10.3390/pr8060665

Gao, J., Zhu, W., Yan, Y., Yue, Z., & Guo, X. (2022). Application of magnetic coagulation for the advanced treatment of ethylene glycol wastewater. *Desalination and Water Treatment*, *246*, 146–155. https://doi.org/10.5004/dwt.2022.28014

Imarah, A. O., Csuka, P., Bataa, N., Decsi, B., Sánta-Bell, E., Molnár, Z., Balogh-Weiser, D., & Poppe, L. (2021). Magnetically

Agitated Nanoparticle-Based Batch Reactors for Biocatalysis with Immobilized Aspartate Ammonia-Lyase. *Catalysts*, *11*(4), 483. https://doi.org/10.3390/catal11040483

Kumar, R., Sabapathy, M., Singh Pawak, V., Ranjan, R., Kakunuri, M., & Veeramani, N. (2026). Nanoparticles for sustainable wastewater treatment: Advances in synthesis, characterization, and remediation applications. *Results in Engineering*, *29*, 109799. https://doi.org/10.1016/j.rineng.2026.109799

Kunduru, K. R., Nazarkovsky, M., Farah, S., Pawar, R. P., Basu, A., & Domb, A. J. (2017). Nanotechnology for water purification: Applications of nanotechnology methods in wastewater treatment. In *Water Purification* (Number January). https://doi.org/10.1016/B978-0-12-804300-4.00002-2

Li, T., Yu, Z., Yang, T., Xu, G., Guan, Y., & Guo, C. (2021). Modified Fe3O4 magnetic nanoparticles for COD removal in oil field produced water and regeneration. *Environmental Technology & Innovation*, *23*, 101630. https://doi.org/10.1016/j.eti.2021.101630

Luo, T., Yang, C., Tian, X., Luo, W., Nie, Y., & Wang, Y. (2021). Application of Iron Oxide Nanomaterials for the Removal of Heavy Metals. *Handbook of Nanomaterials and Nanocomposites for Energy and Environmental Applications: Volumes 1-4*, *3*, 2067–2092. https://doi.org/10.1007/978-3-030-36268-3_76

Marcinowski, P., Bury, D., Krupa, M., Ścieżyńska, D., Prabhu, P., & Bogacki, J. (2020). Magnetite and Hematite in Advanced Oxidation Processes Application for Cosmetic Wastewater Treatment. *Processes*, *8*(11), 1343. https://doi.org/10.3390/pr8111343

Mateus, G. A. P., Dos Santos, T. R. T., Sanches, I. S., Silva, M. F., De Andrade, M. B., Paludo, M. P., Gomes, R. G., & Bergamasco, R. (2020). Evaluation of a magnetic coagulant based on Fe_3O_4 nanoparticles and *Moringa oleifera* extract on tartrazine removal: Coagulation-adsorption and kinetics studies. *Environmental Technology*, *41*(13), 1648–1663. https://doi.org/10.1080/09593330.2018.1543358

Qu, X., Alvarez, P. J. J., & Li, Q. (2013). Applications of nanotechnology in water and wastewater treatment. *Water Research*, *47*(12), 3931–3946. https://doi.org/10.1016/j.watres.2012.09.058

Ramavandi, B. (2014). Treatment of water turbidity and bacteria by using a coagulant extracted from Plantago ovata. *Water Resources and Industry*, *6*, 36–50. https://doi.org/10.1016/j.wri.2014.07.001

Siddiqui, S. I., Alsebaii, N. M., Al-Ghamdi, A. A., Aldahiri, R. H., Alzahrani, E. A., Hafeez, S., Oh, S., & Chaudhry, S. A. (2025). Fe_3O_4/BC for Methylene Blue Removal from Water: Optimization, Thermodynamic, Isotherm, and Kinetic Studies. *Materials*, *18*(9), 2049. https://doi.org/10.3390/ma18092049

Silva, F. M. W. G., Imarah, A. O., Takács, O., Tuba, L., & Poppe, L. (2023). Scalability of U-Shape Magnetic Nanoparticles-Based Microreactor–Lipase-Catalyzed Preparative Scale Kinetic Resolutions of Drug-like Fragments. *Catalysts*, *13*(2). https://doi.org/10.3390/catal13020384

Tetteh, E. K., & Rathilal, S. (2021). Application of magnetized nanomaterial for textile effluent remediation using response surface methodology. *Materials Today: Proceedings*, *38*, 700–711. https://doi.org/10.1016/j.matpr.2020.03.827

Tlili, H., Elaoud, A., Asses, N., Horchani-Naifer, K., Ferhi, M., Goya, G. F., & Fuentes-García, J. A. (2023). Reduction of Oxidizable Pollutants in Waste Water from the Wadi El Bey River Basin Using Magnetic Nanoparticles as Removal Agents. *Magnetochemistry*, *9*(6), 157. https://doi.org/10.3390/magnetochemistry9060157

Waleed Juma, A., Aladdin Jasim, N., & Kharbat Shadhar, A. (2026). Sustainable Green Synthesis of Supported Fe_3O_4 /SiO_2 /$AgVO_3$ Magnetic Nanocomposites for High-Efficiency Removal of Textile Dyes and Recyclable Environmental Remediation. *EPJ Web of Conferences*, *376*, 01005. https://doi.org/10.1051/epjconf/202637601005

Yang, K., Wang, H., Zhou, S., Du, B., & Wang, S. (2026). Recent advancements in Fe_3O_4-based magnetic nanocomposites: Synthesis, adsorption mechanisms, ink pollutants and environmental applications. *Journal of Molecular Structure*, *1351*, 144280. https://doi.org/10.1016/j.molstruc.2025.144280

Yang, T., Gao, C., Guan, Y., & Li, T. (2024). *Facile Preparation of Magnetic Nano-Fe3o4 Modified Powdered Coconut Shell Biochar for Cod Deep Removal in Oil Field Produced Water*. https://doi.org/10.2139/ssrn.4812281

Zakrzewski, W., Dobrzynski, M., Dobrzynski, W., Zawadzka-Knefel, A., Janecki, M., Kurek, K., Lubojanski, A., Szymonowicz, M., Rybak, Z., & Wiglusz, R. J. (2021). Nanomaterials Application in Orthodontics. *Nanomaterials*, *11*(2), 337. https://doi.org/10.3390/nano11020337

Zeng, H., Liu, C., Xu, H., Hao, R., Zhang, J., & Li, D. (2022). Preparation of Fe3O4@C with water treatment residuals and its potential in the magnetic coagulation process. *Journal of Cleaner Production*, *362*, 132327. https://doi.org/10.1016/j.jclepro.2022.132327